

**Divergent regulation of KCNQ1/E1 by targeted recruitment of protein kinase A to distinct sites on the channel complex**

Xinle Zou<sup>1,#</sup>, Sri Karthika Shanmugam<sup>2,#</sup>, Scott A. Kanner<sup>3,#</sup>, Kevin J. Sampson<sup>1</sup>, Robert S. Kass<sup>1</sup>, and Henry M. Colecraft<sup>1,3,4</sup>

<sup>1</sup>Department of Molecular Pharmacology and Therapeutics; <sup>2</sup>Department of Physiology and Cellular Biophysics; <sup>3</sup>Doctoral Program in Neurobiology and Behavior, Columbia University Irving Medical Center, New York, NY

# these authors contributed equally to the work

<sup>4</sup>Correspondence: Henry M. Colecraft  
Department of Physiology and Cellular Biophysics  
Columbia University, College of Physicians and Surgeons  
504 Russ Berrie Pavilion  
1150 St. Nicholas Avenue  
New York, NY 10032  
Phone: 212-851-5372  
Email: [hc2405@cumc.columbia.edu](mailto:hc2405@cumc.columbia.edu)

## Abstract

The slow delayed rectifier potassium current,  $I_{Ks}$ , conducted through pore-forming Q1 and auxiliary E1 ion channel complexes is important for human cardiac action potential repolarization. During exercise or fright,  $I_{Ks}$  is up-regulated by protein kinase A (PKA)-mediated Q1 phosphorylation to maintain heart rhythm and optimum cardiac performance. Sympathetic upregulation of  $I_{Ks}$  requires recruitment of PKA holoenzyme (two regulatory- RI or RII- and two catalytic C $\alpha$  subunits) to Q1 C-terminus by an A kinase anchoring protein (AKAP9). Mutations in Q1 or AKAP9 that abolish their functional interaction result in long QT syndrome type 1 and 11, respectively, which increases the risk of sudden cardiac death during exercise. Here, we investigated the utility of a targeted protein phosphorylation (TPP) approach to reconstitute PKA regulation of  $I_{Ks}$  in the absence of AKAP9. Targeted recruitment of endogenous C $\alpha$  to E1-YFP using a GFP/YFP nanobody (nano) fused to RII $\alpha$  enabled acute cAMP-mediated enhancement of  $I_{Ks}$ , reconstituting physiological regulation of the channel complex. By contrast, nano-mediated tethering of RII $\alpha$  or C $\alpha$  to Q1-YFP constitutively inhibited  $I_{Ks}$  by retaining the channel intracellularly in the endoplasmic reticulum and Golgi. Proteomic analysis revealed distinct phosphorylation sites are modified by C $\alpha$  targeted to Q1-YFP compared to free C $\alpha$ . Thus, functional outcomes of synthetically recruited PKA on  $I_{Ks}$  regulation is critically dependent on the site of recruitment within the channel complex. The results reveal insights into divergent regulation of  $I_{Ks}$  by phosphorylation across different spatial and time scales, and suggest a TPP approach to develop new drugs to prevent exercise-induced sudden cardiac death.

## Introduction

Regulating protein functional expression by targeted induced proximity of enzymes (TIPE) is a burgeoning field with great promise for developing therapeutics to conventionally undruggable targets. The leading edge of this broad concept has been targeted protein degradation (TPD) with small-molecule proteolysis targeting chimeras (PROTACs) which work by recruiting endogenous E3 ubiquitin ligases to chosen proteins<sup>1-3</sup>. Recent promising phase I and II clinical trials of targeted protein degraders represent a realization of the potential of the overall TIPE approach<sup>4</sup>. Beyond targeted protein degradation, there have been nascent efforts to expand the TIPE concept to other physiologically important enzyme classes, including; targeted protein stabilization (TPS) via recruitment of deubiquitinases<sup>5,6</sup>, targeted dephosphorylation using induced proximity of a phosphatase (PhosTACs)<sup>7</sup>, lysosome targeting chimeras (LYTACs) that enable degradation of extracellular proteins<sup>8</sup>, and targeted protein acetylation<sup>9</sup>.

Posttranslational regulation of proteins by phosphorylation is a prominent mechanism for regulating cell biology and physiology that is timely for adaptation to the TIPE idea and has been broached with the development of PhosTACs<sup>7</sup> and phosphorylation inducing chimeric small molecules (PHICS)<sup>10</sup>. The human genome contains ~500 kinases most of which phosphorylate hydroxyl groups on either serine/threonine or tyrosine residues in proteins<sup>11</sup>. Site-specific phosphorylation of proteins can lead to diverse outcomes including; multidimensional regulation of functional activity<sup>12</sup>, protein-protein interactions<sup>13,14</sup>, protein stability<sup>15</sup>, and sub-cellular localization<sup>13,16,17</sup>. Moreover, individual proteins typically have multiple residues that may be phosphorylated raising the possibility of actuating distinctive functional outcomes depending on the particular complement of serine, threonine or tyrosine residues modified under different conditions<sup>12</sup>. Induced recruitment of a kinase to a target may potentially be used to either reconstitute physiologically cognate responses or to realize *de novo* synthetic regulation of protein activity. Overall, by comparison to TPD or stabilization, regulating proteins by targeted protein phosphorylation (TPP) is a potentially more complex prospect, requiring deeper insights into the rules required to achieve specific desired outcomes.

Here, we explore these dimensions of targeted protein phosphorylation by focusing on a cardiac ion channel comprised of pore-forming Q1 and auxiliary E1 subunits. In human heart, Q1/E1 channels give rise to the slowly activating delayed rectifier potassium current,  $I_{Ks}$ , which is essential for normal cardiac action potential repolarization<sup>18</sup>. During sympathetic activation of the heart that occurs during exercise or the fight-or-flight response,  $\beta$ -adrenergic up-regulation of  $I_{Ks}$  occurs via protein kinase A-mediated phosphorylation of Q1 on N-terminus serine residues (Ser27 and Ser92)<sup>19-21</sup>. This effect is crucial to counterbalance the increase in L-type calcium current, that also occurs during sympathetic activation of the heart, to maintain the action potential duration in an appropriate range<sup>22-24</sup>. Loss-of-function mutations in KCNQ1 cause long QT syndrome type 1 (LQT1) due to an increase in the action potential duration that is exacerbated in exercise, thereby elevating the risk of ventricular tachycardias (torsade de pointes) and sudden cardiac death<sup>25</sup>.  $\beta$ -adrenergic regulation of  $I_{Ks}$  is critically dependent on the A kinase anchoring protein, AKAP9 (yotiao), which binds to the C-terminus of Q1 and acts as a scaffold to recruit PKA holoenzyme (comprised of two regulatory RI or RII and two catalytic C $\alpha$  subunits) to the channel complex<sup>20</sup>. Several LQT1 mutations in Q1 C-terminus occur along the binding interface with AKAP9 and may disrupt this crucial protein-protein interaction<sup>20,26-28</sup>. Moreover, mutations in AKAP9 that diminish the interaction with Q1 act as genetic modifiers of LQT1 and cause LQT11<sup>25,29</sup>.

We hypothesized that we could exploit TIPE to reconstitute PKA-mediated regulation of  $I_{Ks}$  in the absence of AKAP9. If successful, this could pave the way to development of PHICS as therapeutics for LQTS. We utilized an anti-GFP nanobody (nano) to direct PKA RII $\alpha$  or C $\alpha$  subunits to YFP-tagged Q1/E1 channel complexes. Targeted recruitment of endogenous C $\alpha$  to E1-YFP using nanoRII $\alpha$  fusion protein enabled acute PKA-mediated enhancement of  $I_{Ks}$ , reconstituting the physiological regulation of the channel complex. Simply overexpressing free C $\alpha$  constitutively recapitulated PKA phosphorylation of Q1 and functional regulation of  $I_{Ks}$  which were not further enhanced by targeting nanoC $\alpha$  to E1-YFP. In sharp contrast, nano-mediated tethering of either RII $\alpha$  or C $\alpha$  to Q1-YFP eliminated  $I_{Ks}$  by retaining Q1 intracellularly in the endoplasmic reticulum (ER) and Golgi compartments. Thus, functional outcomes of synthetically recruited PKA on  $I_{Ks}$  regulation is critically dependent on the site of recruitment within the Q1/E1 channel complex.

## Results

### Targeting RII $\alpha$ to E1 reconstitutes acute PKA modulation of $I_{Ks}$ , whereas anchoring it to Q1 inhibits basal current

We reconstituted  $I_{Ks}$  by co-expressing Q1 + E1 in Chinese hamster ovary (CHO) cells. To examine whether the reconstituted currents are modulated by acute PKA activation, we measured the time course of  $I_{Ks}$  amplitude after breakthrough to the whole-cell configuration with intracellular solution  $\pm$  cAMP/okadaic acid in the patch pipette. In control cells expressing Q1 + E1-YFP + naked nanobody (nano) (Figure 1A), exemplar  $I_{Ks}$  did not increase when compared between immediately after breakthrough and three minutes after dialysis with patch pipette solution either lacking (control) or containing cAMP/OA (Figure 1B). In diary plots of population data, control cells showed a monotonic rundown of  $I_{Ks}$  amplitude that was similar between whether the patch solution contained cAMP/OA or not (Figure 1C). These results are consistent with previously published work showing that acute PKA regulation of  $I_{Ks}$  does not occur in heterologous cells in the absence of co-expressed AKAP9 (yotiao)<sup>20</sup>.

We sought to determine whether we could utilize a nanobody-based targeted recruitment approach to reconstitute acute cAMP-induced PKA regulation of  $I_{Ks}$  independent of AKAP9. To enable recruitment of endogenous C $\alpha$  in a configuration where it is basally inactive and can be acutely activated by cAMP near the channel complex, we fused anti-GFP nanobody to the regulatory subunit (RII $\alpha$ ) of PKA to generate nanoRII $\alpha$ . In cells expressing Q1 + E1-YFP + nanoRII $\alpha$  (Figure 1D), exemplar  $I_{Ks}$  did not show an increase in current amplitude after breakthrough to the whole-cell configuration if the pipette solution lacked cAMP/OA (Figure 1E, *left*). In sharp contrast, when cAMP/OA was present in the patch pipette, exemplar  $I_{Ks}$  displayed a significant increase in current after three minutes of dialysis with intracellular solution (Figure 1E, *right*). In population time course data, the temporal evolution of normalized current amplitude displayed a clear-cut divergence between recordings obtained with or without cAMP/OA in the patch pipette solution ( $I_{3min}/I_0 = 0.9615 \pm 0.025$ ,  $n = 14$  for Q1 + E1-YFP + nanoRII $\alpha$  without cAMP + OA;  $I_{3min}/I_0 = 1.0812 \pm 0.030$ ,  $n = 12$ , for Q1 + E1-YFP + nanoRII $\alpha$  with cAMP + OA;  $P = 0.0054$ , unpaired t-test.) (Figure 1F). The magnitude of the observed response in the diary plots is comparable to the normalized enhancement of  $I_{Ks}$  current observed with cAMP + OA in cells expressing Q1 + E1 + AKAP9<sup>30</sup>. Controls were measured interleaved with the experiment group. In additional control experiments, cells expressing untagged Q1 + E1 +



nanoR11 $\alpha$  displayed no increase or divergence in  $I_{Ks}$  amplitude between recordings in the absence or presence of cAMP/OA in the patch pipette solution (Figure 1 – figure supplement 1). Overall, these data demonstrate successful reconstitution of acute PKA regulation of  $I_{Ks}$  by using a nanobody to tether the regulatory R11 $\alpha$  subunit to E1-YFP in the channel complex.

Does the site of PKA recruitment to the Q1/E1 channel complex matter with respect to functional outcomes? To address this question, we attached YFP to Q1 C-terminus instead of E1 and co-expressed the channel with either naked nanobody (control; nano) or nanoR11 $\alpha$  (Figure 1G). Control cells expressing Q1-YFP + E1 + nano displayed robust basal  $I_{Ks}$  (Figure 1H). Unexpectedly, co-expressing nanoR11 $\alpha$  with Q1-YFP/E1 yielded a substantially suppressed basal  $I_{Ks}$ , suggesting that the site of PKA recruitment to the channel complex is critical in determining functional outcomes (Figure 1, H and I).

### **Targeting PKA-C $\alpha$ to either Q1 or E1 with a nanobody yields divergent functional outcomes on reconstituted $I_{Ks}$**

AKAP9 enables acute PKA regulation of  $I_{Ks}$  by acting as a scaffold that increases the effective local concentration of PKA holoenzyme in the vicinity of the channel complex<sup>20,31</sup>. Accordingly, we wondered whether simply over-expressing free C $\alpha$  would suffice to reconstitute aspects of PKA regulation of  $I_{Ks}$ . Indeed, Western blotting indicated that co-expressing C $\alpha$  led to an increase in Q1 phosphorylation (normalized pQ1/Q1 is increased 1.516-fold for cell expressing C $\alpha$  compared to control) (Figure 2, A and B). Next, we compared key gating parameters of currents recorded from CHO cells expressing Q1 + E1-YFP, either with or without C $\alpha$  co-expression. Current vs voltage ( $I$ - $V$ ) curves indicated that by comparison to currents obtained with Q1 + E1-YFP alone, those recorded from cells co-expressing C $\alpha$  displayed a hyperpolarizing shift in the voltage-dependence activation ( $V_{0.5,act} = 34.5 \pm 3.6$  mV,  $n = 13$  for Q1 + E1-YFP and  $V_{0.5,act} = 25.0 \pm 2.7$ ,  $n = 13$  for Q1 + E1-YFP + C $\alpha$ ,  $P = 0.02$ , unpaired  $t$  test) (Figure 2C), and a trend towards a slower rate of tail current deactivation (in the presence of yotiao) (Figure 2D), two signatures of PKA regulation of  $I_{Ks}$  that is mediated via phosphorylation of Ser27 in Q1<sup>20,32</sup>. Consistent with this, Q1[S27A] reversed the trend towards C $\alpha$ -induced decreased rate of tail current deactivation observed with wild-type Q1 (Figure 2D).

With the impact of free C $\alpha$  as a baseline, we next assessed how nanobody-mediated recruitment of C $\alpha$  to either E1 or Q1 would impact reconstituted  $I_{Ks}$ . We fused C $\alpha$  to anti-GFP nanobody to generate nanoC $\alpha$  and co-expressed it with Q1 + E1-YFP. In this configuration, C $\alpha$  is recruited to the tagged E1 subunit in the channel complex (Figure 2E), as confirmed in a pull-down assay (Figure 2 – figure supplement 1). Compared to control cells expressing Q1 + E1-YFP + nano, channels co-expressed with nanoC $\alpha$  displayed an increased phosphorylation of Q1 (normalized pQ1/Q1 is increased 2.2-fold in cells co-expressing nanoC $\alpha$  compared to controls expressing nano) (Figure 2F), a leftward shift in the voltage-dependence of activation ( $V_{0.5,act} = 34.1 \pm 4.4$  mV,  $n = 10$  for Q1 + E1-YFP + nano and  $V_{0.5,act} = 25.2 \pm 3.4$ ,  $n = 10$  for Q1 + E1-YFP + nanoC $\alpha$ ,  $p = 0.049$ , unpaired,  $t$  test) (Figure 2G), and a trend towards a small augmentation of basal current amplitude ( $I_{avg} = 232.1 \pm 36.44$  mV,  $n = 11$  for Q1 + E1-YFP + nano and  $I_{avg} = 267.24 \pm 37.12$ ,  $n = 16$  for Q1 + E1-YFP + nanoC $\alpha$ ,  $P = 0.5054$ ) (Figure 2H). By contrast, recruiting C $\alpha$  to Q1 (Q1-YFP + E1 + nanoC $\alpha$ ) resulted in a drastic elimination of  $I_{Ks}$  (Figure 2J). To ascertain that the observed effect is due to the activity of the targeted kinase, we introduced a T198A mutation into C $\alpha$  that renders it catalytically dead. Co-expressing nanoC $\alpha$ [T198A] with KCNQ1-YFP/KCNE1 yielded robust currents that were similar in amplitude to control (nano), indicating that intact kinase activity is necessary for the inhibitory effect

observed with nanoCα (Figure 2K). Co-expressing nanoCα with TASK-4-GFP, a two-pore domain K<sup>+</sup> channel, did not decrease whole-cell current density compared to control (Figure 2 – figure supplement 2). Thus, nanoCα does not indiscriminately inhibit currents when recruited to the C-terminus of K<sup>+</sup> channel pore-forming subunits.

### Recruiting Cα or RIIα to either E1 or Q1 yields distinctive effects on channel trafficking

To distinguish the mechanisms underlying the differential functional impact of nanoRIIα and nanoCα on  $I_{Ks}$  depending on whether they are targeted to either E1 or Q1, we assessed their effects on channel trafficking to the cell surface under different conditions. We used a Q1 construct incorporating a high affinity bungarotoxin binding site (BBS) in the extracellular S1-S2 loop to permit detection of channels at the surface in non-permeabilized cells with Alexa Fluor-647 conjugated α-bungarotoxin (BTX-647)<sup>26,33</sup> (Figure 3A). Control cells expressing BBS-Q1 + E1 + nano (in a P2A-CFP construct) displayed robust surface fluorescence as indicated by flow cytometry detection of BTX-647 and CFP (marker for nano expression) fluorescence signals. Co-expressing nanoCα resulted in an elevated BTX-647 fluorescence signal (mean<sub>BTX-647</sub> = 1,505.6 ± 79.88 a.u.,  $N = 5$  for BBS-Q1 + E1 + nano; and mean<sub>BTX-647</sub> = 2,864.2 ± 101.44 a.u.,  $N = 5$  for BBS-Q1 + E1 + nanoCα;  $P < 0.001$ , one-way ANOVA and Tukey HSD post-hoc test) indicating an increase in channel surface density, while nanoRIIα had no significant impact (mean<sub>BTX-647</sub> = 1,393 ± 263.82 a.u.,  $N = 5$  for BBS-Q1 + E1 + nanoRIIα) (Figure 3A-D). Next, we examined how tethering of nano, nanoCα, or nanoRIIα to E1-YFP affected channel trafficking. In this configuration, both nanoCα and nanoRIIα resulted in an increase in BTX-647 fluorescence compared to nano control (mean<sub>BTX-647</sub> = 2,083.2 ± 199.60 a.u.,  $N = 5$  for BBS-Q1 + E1-YFP + nano; and mean<sub>BTX-647</sub> = 2,970 ± 142.26 a.u.,  $N = 5$  for BBS-Q1 + E1-YFP + nanoCα; mean<sub>BTX-647</sub> = 2,772.6 ± 80.99 a.u.,  $N = 5$  for BBS-Q1 + E1-YFP + nanoRIIα,  $P < 0.01$ , one-way ANOVA and Tukey HSD post-hoc test) (Figure 3, E-H). Finally, we examined the impact of individually targeting nano, nanoCα, and nanoRIIα directly to Q1-YFP (Figure 3I). Both nanoCα and nanoRIIα led to a dramatic decrease in BTX-647 fluorescence compared to nano control (mean<sub>BTX-647</sub> = 3,830.4 ± 700.03 a.u.,  $N = 5$  for BBS-Q1-YFP + E1 + nano; mean<sub>BTX-647</sub> = 908 ± 132.95 a.u.,  $N = 5$  for BBS-Q1-YFP + E1 + nanoCα; and mean<sub>BTX-647</sub> = 910 ± 344.68 a.u.,  $N = 5$  for BBS-Q1-YFP + E1 + nanoRIIα,  $P < 0.001$ , one-way ANOVA and Tukey HSD post-hoc test) (Figure 3, J-L), indicating that recruiting these PKA subunits to Q1 C-terminus suppresses channel surface density, and rationalizing the inhibitory impact on  $I_{Ks}$ .

### Targeting Cα or RIIα to Q1 retains channels in the ER and Golgi

Given that targeting either Cα or RIIα specifically to Q1 impairs channel surface trafficking (Figure 3 G-I), we hypothesized that the channels remained trapped in intracellular compartments. To determine intracellular localization of the channels localized, we used confocal imaging to examine the sub-cellular localization of Q1-YFP when co-expressed with nano, nanoCα, or nanoRIIα. We co-expressed either mCherry-tagged ER- or Golgi-localizing marker proteins, respectively, under the different experimental conditions. When co-expressed with nano, Q1-YFP showed some fraction present in both the ER (Figure 4A, top row) and Golgi (Figure 4B, top row) compartments, but also clear staining at the surface membrane. By contrast, co-expressing either nanoCα or nanoRIIα significantly increased the co-localization of Q1-YFP with ER-mCherry (Pearson's colocalization coefficient (PCC) = 0.85 ± 0.020,  $n = 9$  for nano; PCC = 0.90 ± 0.015,  $n = 7$  for nanoCα; and PCC = 0.94 ± 0.010,  $n = 8$  for nanoRIIα;  $P = 0.0049$ , one-way ANOVA and Tukey HSD post-hoc test) (Figure 4, A and B) and Golgi-mCherry (PCC = 0.84 ± 0.016,  $n = 9$  for nano; PCC = 0.90 ± 0.012,  $n = 8$  for nanoCα; and PCC = 0.90 ±

0.011,  $n = 6$  for nanoR11 $\alpha$ ;  $P = 0.0065$ , one-way ANOVA and Tukey HSD post-hoc test) (Figure 4, C and D), respectively, with no discernible YFP signal at the cell surface. Thus, targeting C $\alpha$  or R11 $\alpha$  to Q1-YFP leads to increased retention of the channel in the ER and Golgi compartments.

### **Inducible recruitment of nanoC $\alpha$ to Q1 reveals slow temporal regulation of channel trafficking**

We wondered about the kinetics of this newly revealed regulation of channel trafficking brought on by tethering C $\alpha$  or R11 $\alpha$  to Q1 C-terminus. To gain insights into this question we exploited a small molecule-induced heterodimerization strategy, in which rapamycin simultaneously binds to FK506 binding protein (FKBP) and the FKBP–rapamycin binding domain (FRB) of the mammalian target of rapamycin (mTOR),<sup>34,35</sup> to enable acute temporal control of nanoC $\alpha$  recruitment to Q1 C-terminus (Figure 5A). We fused anti-GFP/YFP nanobody to FKBP and C $\alpha$  to FRB and generated an FKBPnano-P2A-FRBC $\alpha$  construct to ensure 1:1 expression of FKBPnano and FRBC $\alpha$  as separate proteins. We transfected HEK293 cells with BBS-Q1-YFP + E1 + FKBPnano-P2A-FRBC $\alpha$  and monitored channel surface density at various time points after adding 1  $\mu$ M rapamycin to heterodimerize FKBP and FRB fusion proteins (Figure 5, A and B). Channel surface density was relatively unchanged from control (pre-rapamycin) at the 20 and 60-minute time points post-rapamycin (Figure 5C). Beyond that time, Q1-YFP surface density steadily declined, reaching 40% of control 20 hours after rapamycin. Concomitant with the time-dependent decrease in channel surface density post-rapamycin, there was a reciprocal increase in YFP fluorescence, suggesting a stabilization of the total Q1 protein (Figure 5D). Consistent with the induced decrease in Q1 surface density, whole-cell patch clamp showed that in cells expressing Q1-YFP + E1 + FKBPnano-P2A-FRB-C $\alpha$  treatment with 1  $\mu$ M rapamycin for 16 hours resulted in a 60% decline in  $I_{Ks}$  density (Figure 5 E,F). In control experiments, rapamycin had no impact on currents from cells expressing Q1-YFP + E1 alone (Figure 5G).

### **Proteomic analysis reveals distinctive phosphorylation of Q1 residues by C $\alpha$ targeted to Q1-YFP compared to free C $\alpha$**

The most parsimonious explanation for the divergent functional effects of C $\alpha$  either targeted to Q1 or expressed free (or targeted to E1) is that the two treatments result in the phosphorylation of distinct complements of Ser and/or Thr residues on Q1. We used liquid chromatography with tandem mass spectrometry (LC-MS/MS) to identify residues on Q1-YFP that are phosphorylated when the channel is co-expressed with nano (basal control), nanoC $\alpha$ , or free C $\alpha$ . Altogether, we identified 19 Ser and Thr residues that were phosphorylated under at least one of the three experimental conditions (Figure 6A and Figure 6 – figure supplement 1). The pattern of modification of these residues fell in one of three categories: 1) Basally phosphorylated with no increase with either nanoC $\alpha$  or free C $\alpha$  [S6, S402, S407, and S409]; 2) low or undetectable basal phosphorylation with increases in modification seen with both nanoC $\alpha$  and free C $\alpha$  co-expression [S92 and S253]; and 3) low or undetectable basal phosphorylation with an increase in modification seen only with nanoC $\alpha$  co-expression [S457, S468, T470, S484, T498, S546, S571, S577, T610, S623, T624, S627, and S644] (Figure 6 – figure supplement 1).

Given the strong impact of nano-C $\alpha$  on tetrameric Q1 trafficking, we deduced that the residue(s) important for the functional effect would present as a substantial fraction (>25%) of

phosphorylated peptide to total peptide ratio with nano-Cα treatment. Normalization of the fraction of phosphorylated peptide suggested three residues of potential interest – (S468, S484, and T624) (Figure 6A). We tested the impact of mutating these three residues to either alanines (3S/A) or phosphomimetic aspartates (3S/D) on baseline trafficking of Q1-YFP and on nanoCα mediated decrease in channel surface density (Figure 6, B and C). In WT BBS-Q1-YFP, nanoCα produced a 40% decrease in channel surface density (mean<sub>BTX-647</sub> = 1,408.25 ± 40.57 a.u., *N* = 4 for WT BBS-Q1-YFP + nano; and mean<sub>BTX-647</sub> = 849 ± 49.57 a.u., *N* = 4 for WT BBS-Q1-YFP + nanoCα; *P* = 0.0003, unpaired *t* test) (Figure 6, B and C). Compared to WT Q1-YFP, 3S-A showed a 27% decrease in the baseline channel surface expression and a substantially reduced response to nanoCα (mean<sub>BTX-647</sub> = 1,023.5 ± 10.99 a.u., *N* = 4 for BBS-Q1[3S/A]-YFP + nano; and mean<sub>BTX-647</sub> = 880 ± 44.15 a.u., *N* = 4 for BBS-Q1[3S/A]-YFP + nanoCα; *P* = 0.063, unpaired *t* test) (Figure 6, B and C). The diminished effect of nanoCα on 3S-A suggests that increased phosphorylation of at least one of the three residues plays a significant role in the impact of nanoCα on WT Q1 surface density. However, the unexpected decreased baseline surface expression of 3S-A suggests a potential positive effect of phosphorylation of at least one of these residues on basal surface density. Consistent with this interpretation, 3S-D showed an intermediate effect with a 19% decrease in baseline surface density compared to WT, and a diminished response to nanoCα (mean<sub>BTX-647</sub> = 1,023.5 ± 10.99 a.u., *N* = 4 for BBS-Q1[3S/D]-YFP + nano; and mean<sub>BTX-647</sub> = 880 ± 44.15 a.u., *N* = 4 for BBS-Q1[3S/D]-YFP + nanoCα; *P* = 0.063, unpaired *t* test) (Figure 6, B and C). Overall, we conclude that phosphorylation of multiple Ser/Thr residues underlie the large impact of nanoCα targeted to the Q1 C-terminus on channel surface density. Moreover, our results suggest that phosphorylation of distinct Ser/Thr residues may have either a positive or negative impact on channel trafficking, and channel surface density will be determined by a combinatorial contribution of these negative and positive influences.

## Discussion

PKA is known to phosphorylate over 100 distinct substrates in cells, altering protein function to powerfully regulate physiology<sup>36</sup>. In the heart, β-adrenergic agonist activation of PKA results in the increase in contractility and heart rate that underlies the fight-or-flight response. PKA activation increases cardiac L-type currents (*I*<sub>Ca,L</sub>) by phosphorylating the small G-protein Rad which constitutively inhibits a sub-population of Ca<sub>v</sub>1.2 channels in cardiomyocytes<sup>13,37</sup>. Phosphorylation of residues in the Rad C-terminus cause it to disengage from the channel, resulting in augmented *I*<sub>Ca,L</sub> that is critical for the positive inotropic response<sup>13,38</sup>. If unopposed, the PKA-mediated elevated inward *I*<sub>Ca,L</sub> would result in a prolongation of the action potential duration (APD) during exercise or fright<sup>23,24</sup>. This would have two adverse consequences. First, a diminished diastolic period would result in inadequate filling of the heart during diastole, particularly in light of the increased heart rate. Second, the prolonged APD would increase the propensity for lethal cardiac arrhythmias. These injurious sequelae are normally prevented because PKA also increases the amplitude and slows deactivation of *I*<sub>Ks</sub>, providing a countercurrent that serves to maintain a physiologically optimum APD<sup>22-24</sup>. PKA regulation of *I*<sub>Ks</sub> critically depends on the scaffold protein AKAP9 which binds KCNQ1 and anchors the PKA holoenzyme in proximity to the channel<sup>20</sup>. Loss-of-function mutations in KCNQ1 cause long QT syndrome 1 (LQT1), characterized by a prolonged APD and increases susceptibility to exertion triggered lethal cardiac arrhythmias. Some LQT1 mutations occur on the binding interface with

AKAP9, and thus render the channel unable to be regulated in response to  $\beta$ -adrenergic receptor activation<sup>20</sup>. Further, human mutations in AKAP9 that inhibit the interaction with KCNQ1 have been proposed to cause long QT syndrome 11 (LQT11)<sup>25,29</sup>. We show here that the scaffolding function of AKAP9 that enables acute PKA regulation of  $I_{Ks}$  can be supplanted by a nanobody fused to RII $\alpha$  and targeted to E1 in the channel complex. This result suggests a novel approach to develop treatments for LQTS cases arising from disruption of Q1/AKAP9 molecular and/or functional interaction — bivalent small molecules that induce proximity of RII $\alpha$ /RII $\beta$  (or RI) to E1. This approach would require the generation of a nanobody or other antibody-mimetic that binds to the intracellular domain of E1. Beyond  $I_{Ks}$ , diverse AKAPs play an essential role in the proper organization and restriction of PKA signaling to distinct proteins and organelles, and disruption of this capacity leads to serious pathologies<sup>39-41</sup>. Our results suggest a bioengineering approach to rectify such aberrant PKA signaling even in the case of a malfunctioning AKAP.

We surprisingly found that nanoRII $\alpha$  and nanoC $\alpha$  targeted to the C-terminus of Q1 yielded a qualitatively different outcome compared to when they were recruited to E1 C-terminus. The contrasting results illustrate both the challenges and opportunities likely to be encountered in adapting targeted induced proximity of kinases. By contrast with the binary outcomes achieved with the more established targeted protein degradation with PROTACS<sup>1,4</sup>, and more recently targeted protein stabilization<sup>5,6</sup>, PHICS are likely to yield more diverse and nuanced outcomes, in part because the complement of residues modified may depend on the targeting site. The nanobody-based method we have outlined here offers a way to establish the rules that enable a more rational approach to the design and development of PHICS with predicted outcomes. The finding that nanoRII $\alpha$  directed to Q1 C-terminus constitutively inhibited channel trafficking indicates that C $\alpha$  is recruited to the channel complex but not absolutely held in an inactive state under basal conditions. This is most likely due to basal levels of cAMP in the cells being sufficient to bind to nanoRII $\alpha$  tethered to Q1 C-terminus and thereby partially activate PKA to an extent where it can chronically affect channel trafficking. In this configuration, the C $\alpha$  need not dissociate from nanoRII $\alpha$  in order to phosphorylate Q1<sup>42</sup>.

Is the dramatic decrease in channel trafficking and  $I_{Ks}$  induced by nanoC $\alpha$  targeted to Q1 a *de novo* functional property, or is it an amplified version of a naturally occurring phosphate-switch mechanism that controls Q1 surface density? To this point, proteomics analyses indicated several Ser/Thr residues are basally phosphorylated and that this modification is selectively potentiated by nanoC $\alpha$  targeted to Q1, in contrast to free C $\alpha$  expression. Interestingly, examination of the subcellular localization of Q1-YFP indicates expression of the channel in the ER, Golgi, and the plasma membrane. Distinctive regulation of Q1 surface density by kinases has been reported in several previous studies. Activation of protein kinase C (PKC) with phorbol 12-myristate 13-acetate (PMA) decreased  $I_{Ks}$  density by >60% within 30 mins in transfected CHO cells due to Q1/E1 internalization that was dependent on E1 residue S102<sup>43</sup>. Stimulation of  $\alpha_1$  adrenergic receptors produces an acute inhibition of Q1-alone currents (60% reduction in 30 mins) mediated by an internalization of the channel<sup>44</sup>. The mechanism was proposed to involve  $\alpha_1$  adrenergic receptor activation of AMPK which subsequently stimulates Nedd4-2 to increase Q1 ubiquitination and internalization<sup>44</sup>. By comparison with these previously reported forms of kinase-mediated inhibition of Q1 surface density, the mechanism described here is clearly distinct, having a slower time course, and being independent of either E1 expression or Nedd4-2 involvement. The characteristics of the targeted nanoC $\alpha$ /nanoRII $\alpha$ -mediated inhibition of Q1 trafficking are most akin to a reported

chronic down-regulation of  $I_{Ks}$  attributed to a PKC $\epsilon$ -induced reduction in Q1 forward trafficking<sup>45</sup>. We speculate that the chronic targeting of PKA to Q1 C-terminus amplifies a physiological phosphorylation-controlled forward trafficking gate that is normally regulated by another kinase(s) such as potentially, PKC $\epsilon$ .

It is worth noting that there are aspects of AKAP function on  $I_{Ks}$  that we would not expect to be reconstituted with the current configuration of nanoRII $\alpha$ . Beyond acting as a mere scaffold, binding of AKAP9 to Q1 itself has been shown to modulate channel gating downstream of PKA phosphorylation<sup>30</sup>. Further, in addition to anchoring PKA, AKAPs typically serve as hubs that tether other enzymes including phosphatases and phosphodiesterases that influence spatiotemporal aspects of kinase action on substrates<sup>39</sup>. AKAP9 binds to the Q1 C-terminus and would thus tether the PKA holoenzyme to this site in the channel complex<sup>20</sup>. Yet, Q1/E1/AKAP9 complexes are not absolutely retained intracellularly, unlike what we observe for nanoC $\alpha$ , and to a lesser extent for nanoRII $\alpha$ , targeted to Q1-YFP. One possibility to account for the apparent discrepancy is that a phosphatase anchored near Q1 by AKAP9 rapidly dephosphorylates residues that when phosphorylated result in channel retention. Alternatively, the relatively large size of AKAP9 (453 kDa) could position the PKA holoenzyme in a geometrically unfavorable configuration to phosphorylate residues involved in the channel intracellular retention response.

Overall, our findings advance the notion of targeted phosphorylation by recruitment of kinases as a versatile mechanism to control protein function as potent research tools or potential therapeutics. Exploring the numerous potential applications of this iteration of TIPE technology is an interesting prospect for future experiments.

## Acknowledgements

We thank Dr. Ming Chen for technical support. The work was supported by NIH grants R01 HL142111 and R01 HL122421 (to H.M.C) and R01 GM109763 (to R.S.K). S.A.K. was supported by a Medical Scientist Training Program grant (T32 GM007367) and NHLBI National Research Service Award (1F30-HL140878). Flow cytometry experiments were performed in CCTI Flow Cytometry Core, supported in part by the NIH (S10RR027050). Confocal images were collected in the HICC Confocal and Specialized Microscopy Shared Resource, supported by the NIH (P30 CA013696).

## Competing Financial Interests

The authors have no competing financial interests to declare.

<b>Key Resources Table</b>				
<b>Reagent type (species) or resource</b>	<b>Designation</b>	<b>Source or reference</b>	<b>Identifiers</b>	<b>Additional information</b>
cell line ( <i>Homo-sapiens</i> )	HEK293	ATCC	RRID:CVCL_0045	Laboratory of Dr. Robert Kass
cell line ( <i>Homo-sapiens</i> )	CHO	ATCC	RRID:CVCL_0214	CHO-K1, ATCC, CCL-61
antibody	anti-Q1 (Rabbit polyclonal)	Alomone	RRID:AB_2040099	IP (1:1000), WB (1:1000)
antibody	anti-PKA (Rabbit monoclonal)	Abcam	Cat# ab76238, RRID:AB_1523259	IP(1:1000) WB (1:1000)
antibody	anti-actin (Rabbit polyclonal)	Abcam	Cat# ab197345	WB (1:2000)
antibody	anti-pQ1 (Rabbit polyclonal)	PMID: 12566567		WB (1:250)
recombinant DNA reagent	BBS-Q1-YFP (plasmid)	PMID: 25344363		
recombinant DNA reagent	BBS-Q1 (plasmid)	PMID: 25344363		
recombinant DNA reagent	Q1-YFP (plasmid)	PMID: 25344363		

recombinant DNA reagent	Q1 (plasmid)	PMID: 25344363		From the lab of William Kobertz
recombinant DNA reagent	E1-YFP (plasmid)	PMID: 25344363		
recombinant DNA reagent	E1 (plasmid)	PMID: 25344363		From the lab of William Kobertz
recombinant DNA reagent	Yotiao (plasmid)	PMID: 15528278		
recombinant DNA reagent	Q1[S27A]-YFP	This paper		Made by site-directed mutagenesis; see Plasmid constructs and mutagenesis
recombinant DNA reagent	nanoCα-P2A-CFP (plasmid)	This paper		Made by gene synthesis (Genewiz) and cloning; see Plasmid constructs and mutagenesis
recombinant DNA reagent	nanoCα[T198A]-P2A-CFP (plasmid)	This paper		Made by site-directed mutagenesis; see Plasmid constructs and mutagenesis
recombinant DNA reagent	Cα-P2A-CFP (plasmid)	This paper		Made by gene synthesis (Genewiz) and cloning; see Plasmid constructs and



				mutagenesis
recombinant DNA reagent	nanoR11 $\alpha$ -P2A-CFP (plasmid)	This paper		Made by gene synthesis (Genewiz) and cloning; see Plasmid constructs and mutagenesis
recombinant DNA reagent	nano-P2A-CFP (plasmid)	PMID: 29256394		
peptide, recombinant protein	Protein A/G Sepharose beads	Rockland	Cat # PAG50-00-0002	
peptide, recombinant protein	$\alpha$ -bungarotoxin, Alexa Fluor 647 conjugate	Thermo Fisher scientific	Cat # B35450	
commercial assay or kit	Quik-Change Site-Directed Mutagenesis Kit	Agilent Technologies	Cat # 200523	
chemical compound, drug	Rapamycin	Sigma	Cat # 553211-1MG	
software, algorithm	FlowJo	FlowJo, LLC	RRID:SCR_008520	
software, algorithm	GraphPad Prism	GraphPad Software Inc.	RRID:SCR_002798	
software, algorithm	Origin	OriginLab Corporation	RRID:SCR_014212	

software, algorithm	PulseFit	HEKA		
------------------------	----------	------	--	--

## Plasmid constructs and mutagenesis

Human Q1, Q1[S27A], E1, Cα, and Yotiao were cloned in pcDNA3.1 (+) vector. Q1-YFP, E1-YFP, and Q1-BBS-YFP were made as previously described<sup>26</sup>. NanoCα and nanoR11α were created by gene synthesis (Genewiz), and featured the coding sequence for GFP nanobody (vhhGFP4)<sup>46</sup> in frame with cDNA for protein kinase A Cα (NM\_002730) and R11α (X14968) subunits, respectively. Cα, nanoCα, nanoR11α fragments were amplified using the polymerase chain reaction (PCR) and cloned into a customized bicistronic expression vector (xx-P2A-CFP)<sup>33</sup>. Q1[S27A] and nanoCα[T198A] mutations were generated using the Quik-Change Lightning Site-Directed Mutagenesis Kit (Agilent Technologies, Santa Clara, CA). All constructs were verified by sequencing.

## Cell culture and transfection

Low-passage-number Chinese hamster ovary (CHO-K1) cells (American Type Culture Collection) were cultured at 37 °C in Ham's F12 medium with 10% fetal bovine serum (FBS) and 100 µg/mL of penicillin-streptomycin. Cells were transiently transfected with desired plasmids including Q1, Q1[S27A], Q1-YFP, E1, E1-YFP, Cα, nanoCα, nanoR11α, nanoCα[T198A], and Yotiao in 25 cm<sup>2</sup> flask. HEK 293 (RRID:CVCL\_0045) cells were maintained in DMEM medium with 10% fetal bovine serum (FBS) and 100 µg/mL of penicillin-streptomycin. HEK 293 cells and CHO cells were transiently transfected with desired plasmids for Western blot or flow cytometry. Lipofectamine and Plus reagent (Invitrogen) were used for transfection. The cell lines used have been authenticated by STR profiling and determined to be mycoplasma-free using the MycoFluor Mycoplasma Detection Kit (Invitrogen, Carlsbad, CA).

## Western blot

CHO cells cultured in 35mm dishes were transfected with designed plasmids, such as Q1, E1-YFP, Cα and nanoCα, (total DNA is 2.5 µg). Two days after transfection, cells were lysed in a lysis buffer (150 mM NaCl<sub>2</sub>, 1 mM EDTA, 10 mM Tris, 1% Triton X-100, pH 7.5). Cell lysates were resolved by 4-20% SDS-PAGE. Phosphorylated Q1 channels were detected by using the rabbit anti-phosphoQ1 antibody (1:250) and visualized by chemiluminescence with the ECL-plus Western blotting detection system (Amersham Pharmacia). Rabbit anti-Q1 antibody (1:1,000, Alomone labs, Israel) and rabbit anti-actin antibody (1:2000, Abcam, USA) were used to detect total Q1 channels or actin protein in the lysate.

## Electrophysiology

Cells were plated in 3.5 cm culture dishes on the stage of an inverted microscope (OLYMPUS BH2-HLSH, Precision Micro Inc., Massapequa, NY). Currents were recorded at room temperature using the whole cell patch clamp technique by an Axopatch 200B amplifier (Axon Instruments, Foster City, CA). Patch clamp protocols have been described previously<sup>47</sup>. Briefly, after 500 ms of holding potential at -70 mV, the voltage was stepped to +60 mV for 2 seconds and then followed by 2-s repolarizing pulses to -40 mV during which  $I_{Ks}$  tail current was measured (stimulation frequency was 0.06 Hz). External solution contained the following: 132

mM NaCl, 4.8 mM KCl, 2 mM CaCl<sub>2</sub>, 1.2 mM MgCl<sub>2</sub>, 10 mM HEPES and 5 mM glucose (pH was adjusted to 7.4 with NaOH). Internal solution contained the following: 110 mM KCl, 5 mM ATP-K<sub>2</sub>, 11 mM EGTA, 10 mM HEPES, 1 mM CaCl<sub>2</sub> and 1 mM MgCl<sub>2</sub> (pH was adjusted to 7.3 with KOH). Pipette series resistance was typically 1.5 - 3 MΩ when filled with internal solution. Currents were sampled at 10 kHz and filtered at 5 kHz. Traces were acquired at a repetition interval of 10 seconds.

#### **Flow Cytometry assay**

Cell surface and total ion channel pools were assayed by flow cytometry in live, transfected HEK293 cells as previously described<sup>26,33,48</sup>. Briefly, 48 h post-transfection, cells cultured in 12-well plates were gently washed with ice cold PBS containing Ca<sup>2+</sup> and Mg<sup>2+</sup> (in mM: 0.9 CaCl<sub>2</sub>, 0.49 MgCl<sub>2</sub>, pH 7.4), and then incubated for 30 min in blocking medium (DMEM with 3% BSA) at 4°C. The cells were then incubated with 1 μM Alexa Fluor 647 conjugated α-bungarotoxin (BTX-647; Life Technologies) in DMEM/3% BSA on a rocker at 4°C for 1 h, followed by washing three times with PBS (containing Ca<sup>2+</sup> and Mg<sup>2+</sup>). Cells were gently harvested in Ca<sup>2+</sup>-free PBS, and assayed by flow cytometry using a BD LSRII Cell Analyzer (BD Biosciences, San Jose, CA, United States). CFP- and YFP-tagged proteins were excited at 407 and 488 nm, respectively, and Alexa Fluor 647 was excited at 633 nm.

#### **Confocal imaging**

HEK293 cells transfected with enhanced yellow fluorescent protein (EYFP)-tagged KCNQ1 and subcellular marker proteins for ER or Golgi (mCherry-tagged) with either nano, nanoCα or nanoR11α with CFP marker were analyzed 24-48 h after transfection using an inverted Nikon Eclipse Ti microscope equipped with a ×100 objective (Plan Apo VC ×100 Oil DIC N2, Nikon). Images were acquired and analyzed with NIS Elements AR 4 software (Nikon).

#### **Western blot and proteomics sample preparation**

HEK293/CHO cells were washed once with PBS without Ca<sup>2+</sup>, harvested, and resuspended in RIPA lysis buffer containing (in mM) Tris (20, pH 7.4), EDTA (1), NaCl (150), 0.1% (wt/vol) SDS, 1% Triton X-100, 1% sodium deoxycholate and supplemented with protease inhibitor mixture (10 μL/ mL, Sigma-Aldrich, St. Louis, MO), PMSF (1 mM, Sigma-Aldrich) and phosphate inhibitor (.). Lysates were prepared by incubation at 4°C for 1 hr, with occasional vortex, and cleared by centrifugation (10,000 × g, 10 min, 4°C). Supernatants were transferred to new tubes, with aliquots removed for quantification of total protein concentration determined by the bis-cinchonic acid protein estimation kit (Pierce Technologies, Waltham, MA).

For immunoprecipitation, lysates were pre-cleared by incubation with 20 μL Protein A/G Sepharose beads (Rockland) bound to anti-Rabbit IgG (Sigma) for 3h at 4°C. Equivalent total protein amounts were added to spin-columns containing 75 μL Protein A/G Sepharose beads incubated with 4 μg anti-Q1 (Alomone, Jerusalem, Israel), tumbling overnight at 4°C. Immunoprecipitates were washed 3–5 times with RIPA buffer, spun down at 500 × g, eluted with 40 μL of warmed sample buffer [50 mM Tris, 10% (vol/vol) glycerol, 2% SDS, 100 mM DTT, and 0.2 mg/mL bromophenol blue], and boiled (55°C, 15 min). Proteins were resolved on a 4–12% Bis-Tris gradient precast gel (Life Technologies) in MOPS-SDS running buffer (Life Technologies) at 200 V constant for ~1 hr. We loaded 10 μL of the PageRuler Plus Prestained Protein Ladder (10–250 kDa, Thermo Fisher, Waltham, MA) alongside the samples.

For proteomic analysis, the gels were stained with SimplyBlue (ThermoFisher Scientific) and Q1 monomer and dimer bands were excised. In-gel digestion was performed as previously described<sup>49</sup> with minor modifications. Gel slices were washed with 1:1 Acetonitrile and 100 mM ammonium bicarbonate for 30 min then dehydrated with 100% acetonitrile for 10 min until shrunk. The excess acetonitrile was removed, gel slices were dried in speed-vacuum at room temperature for 10 minutes and then reduced with 5 mM DTT for 30 min at 56°C in an air thermostat, cooled down to room temperature, and alkylated with 11 mM IAA for 30 min with no light. Gel slices were then washed with 100 mM of ammonium bicarbonate and 100 % acetonitrile for 10 min each. Excess acetonitrile was removed and dried in a speed-vacuum for 10 min at room temperature and the gel slices were re-hydrated in a solution of 25 ng/μl trypsin in 50 mM ammonium bicarbonate for 30 min on ice and digested overnight at 37°C in an air thermostat. Digested peptides were collected and further extracted from gel slices in extraction buffer (1:2 ratio by volume of 5% formic acid: acetonitrile) at high speed, shaking in an air thermostat. The supernatants from both extractions were combined and dried in a speed-vacuum. Peptides were dissolved in 3% acetonitrile/0.1% formic acid.

For Western blotting, protein bands were transferred from the gel by tank transfer onto a nitrocellulose membrane (3.5 hr, 4°C, 30 V constant) in transfer buffer (25 mM Tris pH 8.3, 192 mM glycine, 15% (vol/vol) methanol, and 0.1% SDS). The membranes were blocked with a solution of 5% nonfat milk (BioRad) in tris-buffered saline-tween (TBS-T) (25 mM Tris pH 7.4, 150 mM NaCl, and 0.1% Tween-20) for 1 hr at RT and then incubated overnight at 4°C with primary antibody (rabbit anti-phospho-KCNQ1) at 1:250 dilution in blocking solution. The blots were washed with TBS-T three times for 10 min each and then incubated with secondary horseradish peroxidase-conjugated antibody for 1 hr at RT. After washing in TBS-T, the blots were developed with a chemiluminescent detection kit (Pierce Technologies) and then visualized on a gel imager. Membranes were then stripped with harsh stripping buffer (2% SDS, 62 mM Tris pH 6.8, 0.8% β-mercaptoethanol) at 50°C for 30 min, rinsed under running water for 2 min, and washed with TBST (3x, 10 min). Membranes were pre-treated with 0.5% glutaraldehyde and re-blotted with rabbit anti-KCNQ1 antibody (1:1,000, Alomone labs, Israel) and rabbit anti-actin antibody (1:2000, Abcam, USA).

#### **Liquid chromatography with tandem mass spectrometry (LC-MS/MS)**

Desalted peptides were injected in an EASY-Spray™ PepMap™ RSLC C18 50cm X 75cm ID column (Thermo Scientific) connected to an Orbitrap Fusion™ Tribrid™ (Thermo Scientific). Peptides elution and separation were achieved at a non-linear flow rate of 250 nl/min using a gradient of 5%-30% of buffer B (0.1% (v/v) formic acid, 100% acetonitrile) for 110 minutes with a temperature of the column maintained at 50°C during the entire experiment. The Thermo Scientific Orbitrap Fusion Tribrid mass spectrometer was used for peptide tandem mass spectroscopy (MS/MS). Survey scans of peptide precursors are performed from 350 to 1500 m/z at 120K full width at half maximum (FWHM) resolution (at 200 m/z) with a 2 x 10<sup>5</sup> ion count target and a maximum injection time of 60 ms. The instrument was set to run in top speed mode with 3-second cycles for the survey and the MS/MS scans. After a survey scan, MS/MS was performed on the most abundant precursors, i.e., those exhibiting a charge state from 2 to 6 of greater than 5 x 10<sup>3</sup> intensity, by isolating them in the quadrupole at 1.6 Th. We used Higher-energy C-trap dissociation (HCD) with 30% collision energy and detected the resulting fragments with the rapid scan rate in the ion trap. The automatic gain control (AGC) target for MS/MS was set to 5 x 10<sup>4</sup> and the maximum injection time was limited to 30 ms. The dynamic

exclusion was set to 30 s with a 10 ppm mass tolerance around the precursor and its isotopes. Monoisotopic precursor selection was enabled.

### **LC-MS/MS data analysis**

Raw mass spectrometric data were analyzed using the Proteome Discoverer 2.4 to perform database search and LFQ quantification at default settings. PD2.4 was set up to search with the reference human proteome database downloaded from UniProt and performed the search trypsin digestion with up to 2 missed cleavages. Peptide and protein false discovery rates (FDR) were all set to 1%. The following modifications were used for protein identification and LFQ quantification: Carbamidomethyl(C) was set as fixed modification and variable modifications of Oxidation (M) and Acetyl (Protein N-term), DiGly (K) and deamination for asparagine or glutamine (NQ). Results obtained from PD2.4 were further used to quantify relative phosphorylated peptide abundances under the different conditions and identifying sites modified on KCNQ1.

### **Data Analysis**

Patch clamp data, shown as mean  $\pm$  S.E.M., were acquired using pCLAMP 8.0 (Axon Instruments) and analyzed with Origin 7.0 (OriginLab, Northampton, MA) and Clampfit 8.2 (Axon Instruments). Flow cytometry data were analyzed using FlowJo 10.8 software. Statistical data analysis was assessed with Student's *t*-test for comparison between two groups and one-way ANOVA for comparisons among more than two groups, followed by pairwise comparisons using Tukey HSD post-hoc test. In the Figures, data are shown as mean  $\pm$  S.E.M., and statistically significant differences to control values are indicated by asterisks (\*,  $P < 0.05$ ; \*\*,  $P < 0.01$ ; \*\*\*,  $P < 0.001$ ).

### **Material availability statement**

Plasmid constructs for non-commercial purposes can be obtained by request from the corresponding author after publication of the manuscript.

## Figure Legends

### Figure 1: Differential functional effects of nanoRil $\alpha$ targeted to either KCNE1 or KCNQ1 on $I_{Ks}$

(A) Cartoon showing targeting GFP/YFP nanobody (nano) to Q1/E1 channel complex via a YFP tag on E1. (B) Exemplar  $I_{Ks}$  traces elicited by test pulses (+60 mV, -40 mV return) reconstituted in CHO cells expressing Q1/E1-YFP + nano at 1 min (black traces) or 3 min (red traces) after break-in to whole-cell configuration. Cells were dialyzed with internal solution either lacking (*left*) or including (*right*) 0.2 mM cAMP + 0.2  $\mu$ M okadaic acid (cAMP/OA). (C) Diary plot of population tail-current amplitudes (mean  $\pm$  SEM) vs time with cAMP/OA either lacking (black symbols,  $n = 10$ ) or included (red symbols,  $n = 11$ ) in the patch pipette solution. (D-F) Cartoon, exemplar currents and population tail-current amplitude vs time for CHO cells expressing Q1/E1-YFP + nanoRil $\alpha$ . Same format as (A-C).  $**P < 0.01$ , two-tailed unpaired  $t$  test. (G) Cartoon showing nanoRil $\alpha$  targeting to Q1/E1 channel complex via YFP tag on Q1. (H) Exemplar  $I_{Ks}$  traces reconstituted in CHO cells expressing Q1-YFP/E1 with either nano (*left*) or nanoRil $\alpha$  (*right*). (I) Population current densities (nano,  $n = 26$ ; nanoRil $\alpha$ ,  $n = 17$ ).  $***P < 0.001$ , two-tailed unpaired  $t$  test.

### Figure 1 – source data 1

### Differential functional effects of nanoRil $\alpha$ targeted to either KCNE1 or KCNQ1 on $I_{Ks}$

### Figure 1 – figure supplement 1: NanoRil $\alpha$ does not reconstitute PKA regulation of $I_{Ks}$ when co-expressed with untagged KCNQ1 + KCNE1

(A) Schematic showing nanoRil $\alpha$  co-expressed with Q1/E1 channel complex. (B) Diary plot of population tail-current amplitudes (mean  $\pm$  SEM) vs time with cAMP/OA either lacking (black symbols,  $n = 5$ ) or included (red symbols,  $n = 5 - 9$ ) in the patch pipette solution.

### Figure 1 – figure supplement 1 – source data 1

### NanoRil $\alpha$ does not reconstitute PKA regulation of $I_{Ks}$ when co-expressed with untagged KCNQ1 + KCNE1.

### Figure 2: Differential functional effects of nano-C $\alpha$ targeted to either Q1 or E1 on $I_{Ks}$

(A) Cartoon showing Q1/E1-YFP complex co-expressed with or without free PKA C $\alpha$  subunit. (B) Representative immunoblots of lysates from HEK293 cells co-expressing Q1/E1-YFP with either empty pcDNA3.1 vector or free C $\alpha$ . Anti-pKCNQ1 (top) detects phosphorylated KCNQ1-S27, anti-KCNQ1 (middle) detects total KCNQ1, and anti-Actin (bottom) detects total actin.  $N = 1$ . (C)  $I_{Ks}$  activation curves in CHO cells co-expressing Q1, E1-YFP with either empty pcDNA3.1 vector (black symbols,  $n = 13$ ) or free PKA C $\alpha$  (red symbols,  $n = 13$ ). (D) Tail-decay times for currents recorded from cells co-expressing Q1/E-YFP + yotiao and either nano or free PKA C $\alpha$ , or cells co-expressing Q1[S27A]/E1-YFP + yotiao and free PKA C $\alpha$  ( $P = 0.0532$ , One-way ANOVA). (E-H) Cartoon, immunoblots,  $I_{Ks}$  activation curves, and population current densities of Q1/E1-YFP complex expressed with either nano ( $n = 10$ ) or nanoC $\alpha$  ( $n = 10$ ). (I) Cartoon showing targeting of nanoC $\alpha$  to Q1/E1 complex via YFP tag on Q1 C-terminus. (J) Exemplar

current traces  $I_{Ks}$  traces from CHO cells co-expressing Q1-YFP/E1 with either nanoCa (*left*) or catalytically inactive nanoCa [T198A] mutant (*right*). (K) Population current densities (nano,  $n = 26$ ; nanoCa,  $n = 19$ ; nanoCa[T198A],  $n = 10$ ).

**Figure 2 – source data 1**

**Figure 2 – source data 2**

**Differential functional effects of nano-Ca targeted to either Q1 or E1 on  $I_{Ks}$**

**Figure 2 – figure supplement 1: Evidence that nanoCa but not free PKA Ca is recruited to E1-YFP in the Q1/E1-YFP channel complex.**

Representative immunoblots of lysates from untransfected HEK293 cells (UT) or co-expressing Q1/E1-YFP with either nanoCa or free Ca, immunoprecipitated with anti-PKA Ca and probed with (A) anti-YFP to detect E1-YFP, or (B) anti-PKA Ca to detect nanoCa and free Ca, respectively. (C) Input controls from same samples blotted with anti-YFP. (D) Anti-actin loading controls.  $N = 2$  for each blot.

**Figure 2 – figure supplement 1 – source data 1**

**Figure 2 – figure supplement 2: NanoCa targeted to the C-terminus of TASK1 via a GFP tag does not inhibit  $K^+$  current.**

(A) Exemplar current-voltage relationship elicited by a ramp stimulus (-120 to +60 mV) in a CHO cell expressing hTASK1-GFP + nano. (B) Exemplar current-voltage relationship elicited by a ramp stimulus in a CHO cell expressing hTASK1-GFP + nanoCa. (C) Population current density at 0 mV for cells expressing hTASK1-GFP with either nano (black bar,  $n = 7$ ) or nanoCa (red bar,  $n = 9$ ).

**Figure 2 – figure supplement 2 – source data 1**

**NanoCa targeted to the C-terminus of TASK1 via a GFP tag does not inhibit  $K^+$  current**

**Figure 3: Tethering Ca and RII $\alpha$  to either E1 or Q1 yields differential effects on channel surface density**

(A) Cartoon showing strategy for surface labeling of BBS-Q1/E1 using BTX-647. (B) Flow cytometry contour plots showing surface channels (BTX-647 fluorescence) and nano expression (CFP fluorescence) in cells expressing BBS-Q1/E1 with nano (*left*), nanoCa (*middle*) or nanoRII $\alpha$  (*right*). (C) Corresponding cumulative distribution (CDF) histograms of BTX-647 fluorescence. Plot generated from population of CFP-positive cells. (D) Channel surface density (mean BTX-647 fluorescence in CFP-positive cells). \*  $P = 0.0003$ , one-way ANOVA and Tukey HSD post-hoc test. (E-H) Cartoon, contour plots, CDF and average surface labeling of BBS-Q1 in cells expressing BBS-Q1/E1-YFP with nano, nanoCa or nanoRII $\alpha$ , same format as A-D. #  $P < 0.05$ , one-way ANOVA and Tukey HSD post-hoc test. (I-L) Cartoon, contour plots, CDF and normalized average surface labeling of BBS-Q1-YFP in cells expressing BBS-Q1-YFP/E1 with

nano, nanoCα or nanoR11α, same format as A-D. \*\*  $P < 0.05$ , one-way ANOVA and Tukey HSD post-hoc test.

### Figure 3 – source data 1

### Tethering Cα and R11α to either E1 or Q1 yields differential effects on channel surface density

### Figure 4: Subcellular localization of KCNQ1 tethered to nano, nanoCα, or nanoR11α

(A) Representative confocal images of HEK293 cells expressing Q1-YFP/E1 and ER-mCherry marker with nano, nanoCα or nanoR11α. (B) Co-localization of Q1-YFP with ER-mCherry assessed by Pearson's colocalization coefficient;  $n = 9$  for nano,  $n = 7$  for nanoCα and  $n = 8$  for nanoR11α. (C) Representative confocal images of HEK293 cells expressing Q1-YFP/E1 and Golgi-mCherry marker with nano, nanoCα, or nanoR11α. (D) Co-localization of Q1-YFP with ER-mCherry assessed by Pearson's colocalization coefficient;  $n = 9$  for nano,  $n = 8$  for nanoCα, and  $n = 6$  for nanoR11α. \*  $P < 0.05$ , one-way ANOVA and Tukey HSD post-hoc test).

### Figure 5: Slow temporal regulation of channel trafficking by targeted induced recruitment of nanoCα to Q1 C-terminus

(a) Cartoon of FKBP/FRB heterodimerization strategy utilized for rapamycin-induced recruitment of engineered Cα to BBS-Q1-YFP/E1. (B) Exemplar flow cytometry contour plots showing surface expression (BTX-647 fluorescence) and CFP fluorescence in cells expressing BBS-Q1-YFP/E1 with FRB-Cα and FKBP-nano at times  $t = 0$  (left),  $t = 6$ h (middle) and  $t = 24$ h (right) after rapamycin addition. (c) Normalized mean Q1 surface density (BTX-647 fluorescence) plotted as a function of time after rapamycin induction. (d) Normalized mean Q1 total expression (YFP fluorescence) plotted as a function of time after rapamycin induction. (e) Exemplar  $I_{KS}$  traces recorded in CHO cells co-expressing KCNQ1-YFP/KCNE1/Nano-FKBP-FRB-Cα incubated 20 hours either without (left) or with (right) rapamycin. (f) Mean current densities in CHO cells co-expressing KCNQ1-YFP/KCNE1/Nano-FKBP-FRB-Cα without rapamycin (black,  $n = 10$ ) or after 20 h rapamycin incubation (red,  $n = 14$ ). \*\*\*  $P < 0.001$ , paired  $t$  test. (g) Mean current densities in control cells co-expressing KCNQ1-YFP/KCNE1 without rapamycin (black,  $n = 8$ ) or after 20 h rapamycin incubation (red,  $n = 9$ ).

### Figure 5 – source data 1

### Slow temporal regulation of channel trafficking by targeted induced recruitment of nanoCα to Q1 C-terminus

### Figure 6: Potential phosphorylation sites involved in PKA modulation of KCNQ1 trafficking

(a) Top, schematic of Q1 showing positions of Ser and Thr residues where phosphorylation was increased when nanoCα was targeted to Q1 C-terminus. Bottom, relative abundance of phosphorylated KCNQ1-YFP peptides identified using mass spectrometry in cells co-expressing nano (black), nanoCα (red), or free Cα (cyan). (b) Exemplar CDF plots showing channel surface density in cells expressing WT BBS-Q1-YFP (left), BBS-3S/A-YFP (middle), or BBS-3S/D-YFP



(*right*) in the absence (black traces) or presence (red traces) of nanoCa. (c) Channel surface density (mean BTX-647 fluorescence in YFP-positive cells) in cells expressing WT BBS-Q1-YFP, BBS-3S/A-YFP, or BBS-3S/D-YFP in the presence of either nano or nanoCa. WT BBS-Q1-YFP (nano,  $N = 4$ ; nanoCa,  $N = 4$ ; \*  $P < 0.001$ , unpaired t-test). BBS-3S/A-YFP (nano,  $N = 4$ ; nanoCa,  $N = 4$ ;  $P = 0.063$ , unpaired t-test). BBS-3S/D-YFP (nano,  $N = 4$ ; nanoCa,  $N = 4$ ;  $P = 0.079$ , unpaired t-test). #  $P < 0.001$  compared to WT + nano, one-way ANOVA and Tukey HSD post-hoc test.

**Figure 6 – source data 1**

**Figure 6 – source data 2**

**Potential phosphorylation sites involved in PKA modulation of KCNQ1 trafficking**

**Figure 6 – figure supplement 1**

Relative abundance of phosphorylated KCNQ1-YFP peptides identified using mass spectrometry in cells co-expressing nano (black), nanoCa (red), or free Ca (cyan).

## References

- 1 Sakamoto, K. M. *et al.* Protacs: chimeric molecules that target proteins to the Skp1-Cullin-F box complex for ubiquitination and degradation. *Proc Natl Acad Sci U S A* **98**, 8554-8559, doi:10.1073/pnas.141230798 (2001).
- 2 Schneekloth, J. S., Jr. *et al.* Chemical genetic control of protein levels: selective in vivo targeted degradation. *J Am Chem Soc* **126**, 3748-3754, doi:10.1021/ja039025z (2004).
- 3 Nalawansa, D. A. & Crews, C. M. PROTACs: An Emerging Therapeutic Modality in Precision Medicine. *Cell Chem Biol* **27**, 998-1014, doi:10.1016/j.chembiol.2020.07.020 (2020).
- 4 Bekes, M., Langley, D. R. & Crews, C. M. PROTAC targeted protein degraders: the past is prologue. *Nat Rev Drug Discov* **21**, 181-200, doi:10.1038/s41573-021-00371-6 (2022).
- 5 Kanner, S. A., Shuja, Z., Choudhury, P., Jain, A. & Colecraft, H. M. Targeted deubiquitination rescues distinct trafficking-deficient ion channelopathies. *Nat Methods* **17**, 1245-1253, doi:10.1038/s41592-020-00992-6 (2020).
- 6 Henning, N. J. *et al.* Deubiquitinase-targeting chimeras for targeted protein stabilization. *Nat Chem Biol* **18**, 412-421, doi:10.1038/s41589-022-00971-2 (2022).
- 7 Chen, P. H. *et al.* Modulation of Phosphoprotein Activity by Phosphorylation Targeting Chimeras (PhosTACs). *ACS Chem Biol* **16**, 2808-2815, doi:10.1021/acscchembio.1c00693 (2021).
- 8 Banik, S. M. *et al.* Lysosome-targeting chimeras for degradation of extracellular proteins. *Nature* **584**, 291-297, doi:10.1038/s41586-020-2545-9 (2020).
- 9 Wang, W. W. *et al.* Targeted Protein Acetylation in Cells Using Heterobifunctional Molecules. *J Am Chem Soc* **143**, 16700-16708, doi:10.1021/jacs.1c07850 (2021).
- 10 Siriwardena, S. U. *et al.* Phosphorylation-Inducing Chimeric Small Molecules. *J Am Chem Soc* **142**, 14052-14057, doi:10.1021/jacs.0c05537 (2020).
- 11 Fabbro, D., Cowan-Jacob, S. W. & Moebitz, H. Ten things you should know about protein kinases: IUPHAR Review 14. *Br J Pharmacol* **172**, 2675-2700, doi:10.1111/bph.13096 (2015).
- 12 Cohen, P. The regulation of protein function by multisite phosphorylation--a 25 year update. *Trends Biochem Sci* **25**, 596-601, doi:10.1016/s0968-0004(00)01712-6 (2000).
- 13 Liu, G. *et al.* Mechanism of adrenergic CaV1.2 stimulation revealed by proximity proteomics. *Nature* **577**, 695-700, doi:10.1038/s41586-020-1947-z (2020).
- 14 Pennington, K. L., Chan, T. Y., Torres, M. P. & Andersen, J. L. The dynamic and stress-adaptive signaling hub of 14-3-3: emerging mechanisms of regulation and context-dependent protein-protein interactions. *Oncogene* **37**, 5587-5604, doi:10.1038/s41388-018-0348-3 (2018).
- 15 Xu, C., Kim, N. G. & Gumbiner, B. M. Regulation of protein stability by GSK3 mediated phosphorylation. *Cell Cycle* **8**, 4032-4039, doi:10.4161/cc.8.24.10111 (2009).
- 16 El Amri, M., Fitzgerald, U. & Schlosser, G. MARCKS and MARCKS-like proteins in development and regeneration. *J Biomed Sci* **25**, 43, doi:10.1186/s12929-018-0445-1 (2018).
- 17 Yang, J. W., Vacher, H., Park, K. S., Clark, E. & Trimmer, J. S. Trafficking-dependent phosphorylation of Kv1.2 regulates voltage-gated potassium channel cell surface expression. *Proc Natl Acad Sci U S A* **104**, 20055-20060, doi:10.1073/pnas.0708574104 (2007).
- 18 Sanguinetti, M. C. *et al.* Coassembly of K(V)LQT1 and minK (IsK) proteins to form cardiac I(Ks) potassium channel. *Nature* **384**, 80-83, doi:10.1038/384080a0 (1996).
- 19 Kurokawa, J., Chen, L. & Kass, R. S. Requirement of subunit expression for cAMP-mediated regulation of a heart potassium channel. *Proc Natl Acad Sci U S A* **100**, 2122-2127, doi:10.1073/pnas.0434935100 (2003).
- 20 Marx, S. O. *et al.* Requirement of a macromolecular signaling complex for beta adrenergic receptor modulation of the KCNQ1-KCNE1 potassium channel. *Science* **295**, 496-499, doi:10.1126/science.1066843

295/5554/496 [pii] (2002).

21 Lundby, A. *et al.* In vivo phosphoproteomics analysis reveals the cardiac targets of beta-adrenergic receptor signaling. *Sci Signal* **6**, rs11, doi:10.1126/scisignal.2003506 (2013).

22 Banyasz, T. *et al.* Beta-adrenergic stimulation reverses the I Kr-I Ks dominant pattern during cardiac action potential. *Pflugers Arch* **466**, 2067-2076, doi:10.1007/s00424-014-1465-7 (2014).

23 Volders, P. G. *et al.* Probing the contribution of IKs to canine ventricular repolarization: key role for beta-adrenergic receptor stimulation. *Circulation* **107**, 2753-2760, doi:10.1161/01.CIR.0000068344.54010.B3 (2003).

24 Gadsby, D. C. Beta-adrenoceptor agonists increase membrane K<sup>+</sup> conductance in cardiac Purkinje fibres. *Nature* **306**, 691-693, doi:10.1038/306691a0 (1983).

25 Schwartz, P. J., Crotti, L. & Insolia, R. Long-QT syndrome: from genetics to management. *Circ Arrhythm Electrophysiol* **5**, 868-877, doi:10.1161/CIRCEP.111.962019 (2012).

26 Aromolaran, A. S., Subramanyam, P., Chang, D. D., Kobertz, W. R. & Colecraft, H. M. LQT1 mutations in KCNQ1 C-terminus assembly domain suppress IKs using different mechanisms. *Cardiovasc Res* **104**, 501-511, doi:10.1093/cvr/cvu231 (2014).

27 Tester, D. J., Will, M. L., Haglund, C. M. & Ackerman, M. J. Compendium of cardiac channel mutations in 541 consecutive unrelated patients referred for long QT syndrome genetic testing. *Heart Rhythm* **2**, 507-517, doi:S1547-5271(05)00191-8 [pii] 10.1016/j.hrthm.2005.01.020 (2005).

28 Howard, R. J., Clark, K. A., Holton, J. M. & Minor, D. L., Jr. Structural insight into KCNQ (Kv7) channel assembly and channelopathy. *Neuron* **53**, 663-675, doi:S0896-6273(07)00109-2 [pii] 10.1016/j.neuron.2007.02.010 (2007).

29 Chen, L. *et al.* Mutation of an A-kinase-anchoring protein causes long-QT syndrome. *Proc Natl Acad Sci U S A* **104**, 20990-20995, doi:10.1073/pnas.0710527105 (2007).

30 Kurokawa, J., Motoike, H. K., Rao, J. & Kass, R. S. Regulatory actions of the A-kinase anchoring protein Yotiao on a heart potassium channel downstream of PKA phosphorylation. *Proc Natl Acad Sci U S A* **101**, 16374-16378, doi:10.1073/pnas.0405583101 (2004).

31 Langeberg, L. K. & Scott, J. D. Signalling scaffolds and local organization of cellular behaviour. *Nat Rev Mol Cell Biol* **16**, 232-244, doi:10.1038/nrm3966 (2015).

32 Chen, L., Kurokawa, J. & Kass, R. S. Phosphorylation of the A-kinase-anchoring protein Yotiao contributes to protein kinase A regulation of a heart potassium channel. *J Biol Chem* **280**, 31347-31352, doi:10.1074/jbc.M505191200 (2005).

33 Kanner, S. A., Morgenstern, T. & Colecraft, H. M. Sculpting ion channel functional expression with engineered ubiquitin ligases. *eLife* **6**, doi:10.7554/eLife.29744 (2017).

34 Crabtree, G. R. & Schreiber, S. L. Three-part inventions: intracellular signaling and induced proximity. *Trends Biochem Sci* **21**, 418-422, doi:S0968-0004(96)20027-1 [pii] (1996).

35 Inoue, T., Heo, W. D., Grimley, J. S., Wandless, T. J. & Meyer, T. An inducible translocation strategy to rapidly activate and inhibit small GTPase signaling pathways. *Nat Methods* **2**, 415-418, doi:nmeth763 [pii] 10.1038/nmeth763 (2005).

36 Shabb, J. B. Physiological substrates of cAMP-dependent protein kinase. *Chem Rev* **101**, 2381-2411, doi:10.1021/cr000236l (2001).

37 Finlin, B. S., Crump, S. M., Satin, J. & Andres, D. A. Regulation of voltage-gated calcium channel activity by the Rem and Rad GTPases. *Proc Natl Acad Sci U S A* **100**, 14469-14474, doi:10.1073/pnas.2437756100

2437756100 [pii] (2003).

38 Papa, A. *et al.* Rad regulation of Ca(V)1.2 channels controls cardiac fight-or-flight response. *Nat Cardiovasc Res* **1**, 1022-1038, doi:10.1038/s44161-022-00157-y (2022).

39 Wong, W. & Scott, J. D. AKAP signalling complexes: focal points in space and time. *Nat Rev Mol Cell Biol* **5**, 959-970, doi:10.1038/nrm1527 (2004).

40 Kjallquist, U. *et al.* Exome sequencing of primary breast cancers with paired metastatic lesions reveals metastasis-enriched mutations in the A-kinase anchoring protein family (AKAPs). *BMC Cancer* **18**, 174, doi:10.1186/s12885-018-4021-6 (2018).

41 Gold, M. G., Gonen, T. & Scott, J. D. Local cAMP signaling in disease at a glance. *J Cell Sci* **126**, 4537-4543, doi:10.1242/jcs.133751 (2013).

42 Smith, F. D. *et al.* Local protein kinase A action proceeds through intact holoenzymes. *Science* **356**, 1288-1293, doi:10.1126/science.aaj1669 (2017).

43 Kanda, V. A., Purtell, K. & Abbott, G. W. Protein kinase C downregulates I(Ks) by stimulating KCNQ1-KCNE1 potassium channel endocytosis. *Heart Rhythm* **8**, 1641-1647, doi:10.1016/j.hrthm.2011.04.034 (2011).

44 Kurakami, K. *et al.* KCNQ1 is internalized by activation of alpha1 adrenergic receptors. *Biochem Pharmacol* **169**, 113628, doi:10.1016/j.bcp.2019.113628 (2019).

45 Gou, X. *et al.* Specific protein kinase C isoform exerts chronic inhibition on the slowly activating delayed-rectifier potassium current by affecting channel trafficking. *Channels (Austin)* **15**, 262-272, doi:10.1080/19336950.2021.1882112 (2021).

46 Kubala, M. H., Kovtun, O., Alexandrov, K. & Collins, B. M. Structural and thermodynamic analysis of the GFP:GFP-nanobody complex. *Protein Sci* **19**, 2389-2401, doi:10.1002/pro.519 (2010).

47 Terrenoire, C., Houslay, M. D., Baillie, G. S. & Kass, R. S. The cardiac IKs potassium channel macromolecular complex includes the phosphodiesterase PDE4D3. *J Biol Chem* **284**, 9140-9146, doi:10.1074/jbc.M805366200 (2009).

48 Kanner, S. A., Jain, A. & Colecraft, H. M. Development of a High-Throughput Flow Cytometry Assay to Monitor Defective Trafficking and Rescue of Long QT2 Mutant hERG Channels. *Frontiers in physiology* **9**, 397, doi:10.3389/fphys.2018.00397 (2018).

49 Shevchenko, A., Tomas, H., Havlis, J., Olsen, J. V. & Mann, M. In-gel digestion for mass spectrometric characterization of proteins and proteomes. *Nat Protoc* **1**, 2856-2860, doi:10.1038/nprot.2006.468 (2006).

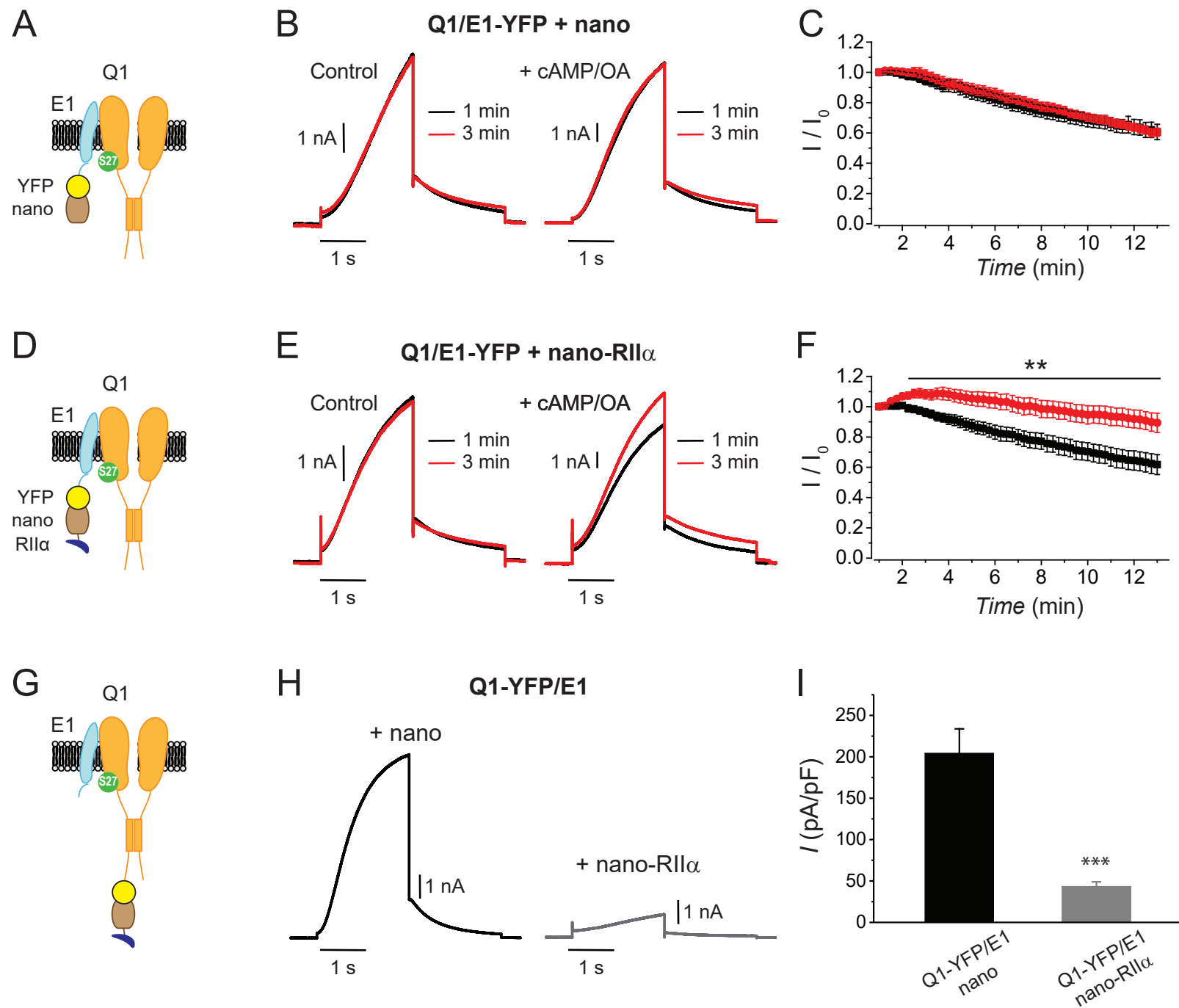


FIGURE 1

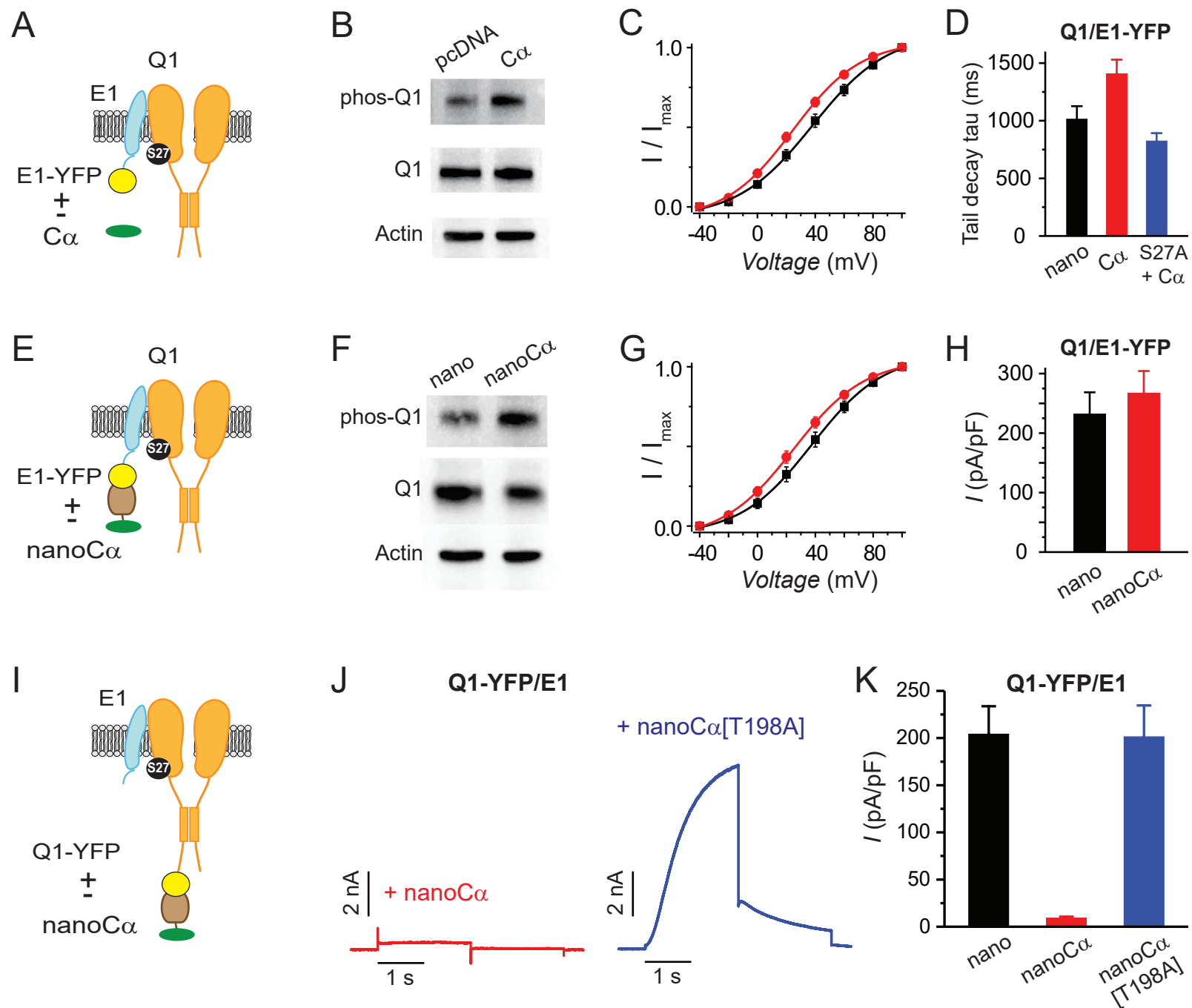


FIGURE 2

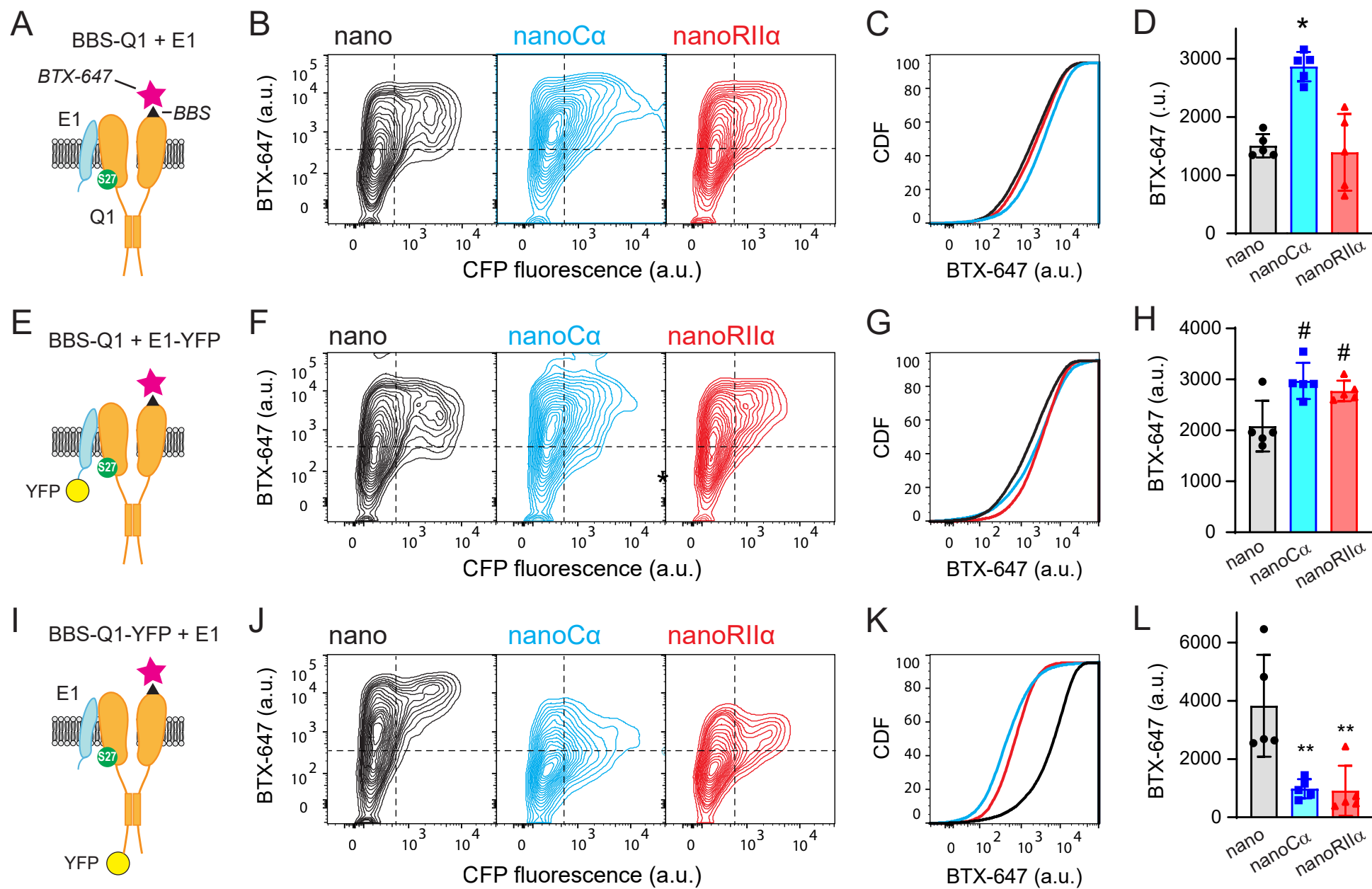


FIGURE 3

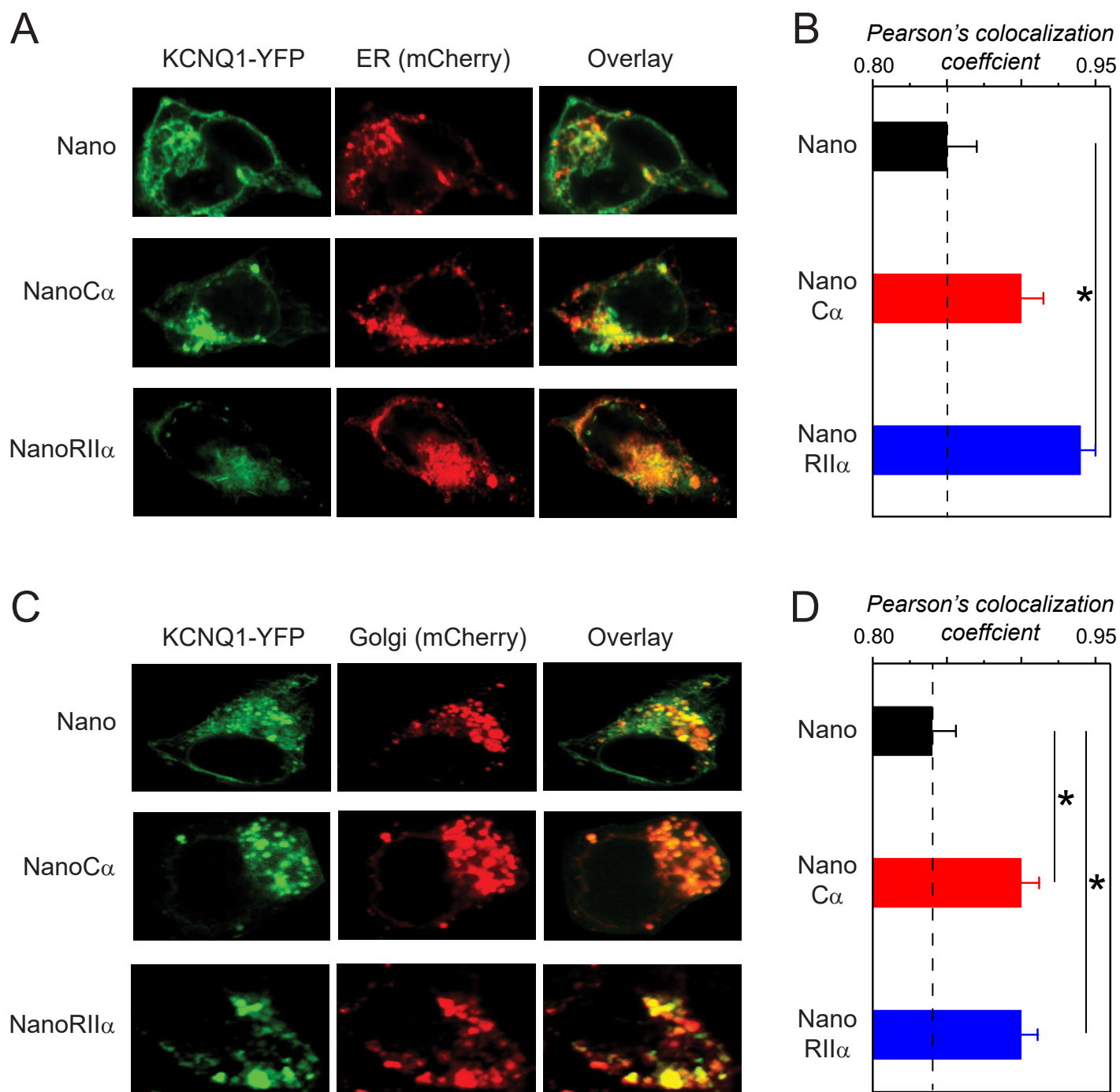


FIGURE 4



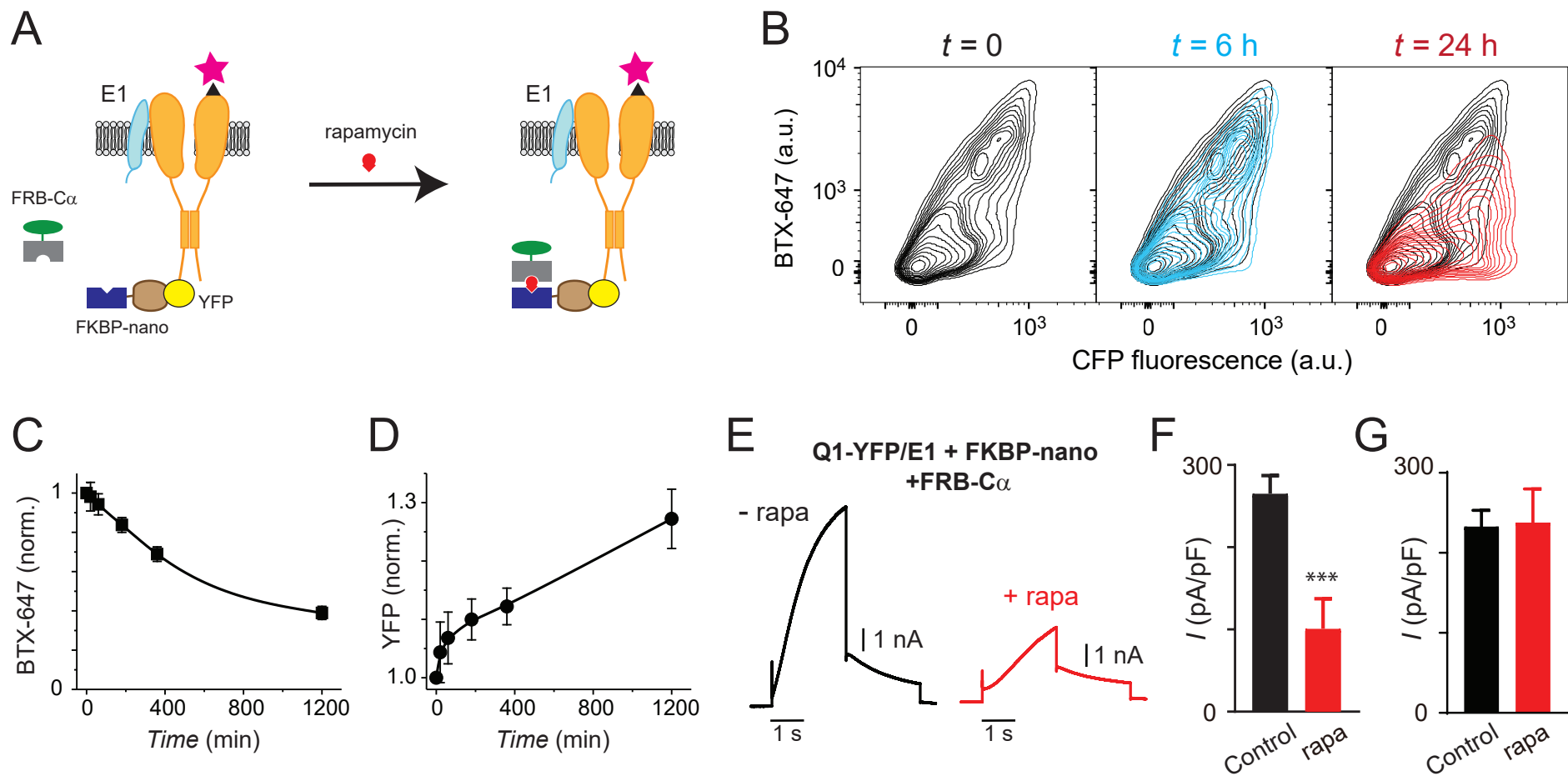


FIGURE 5

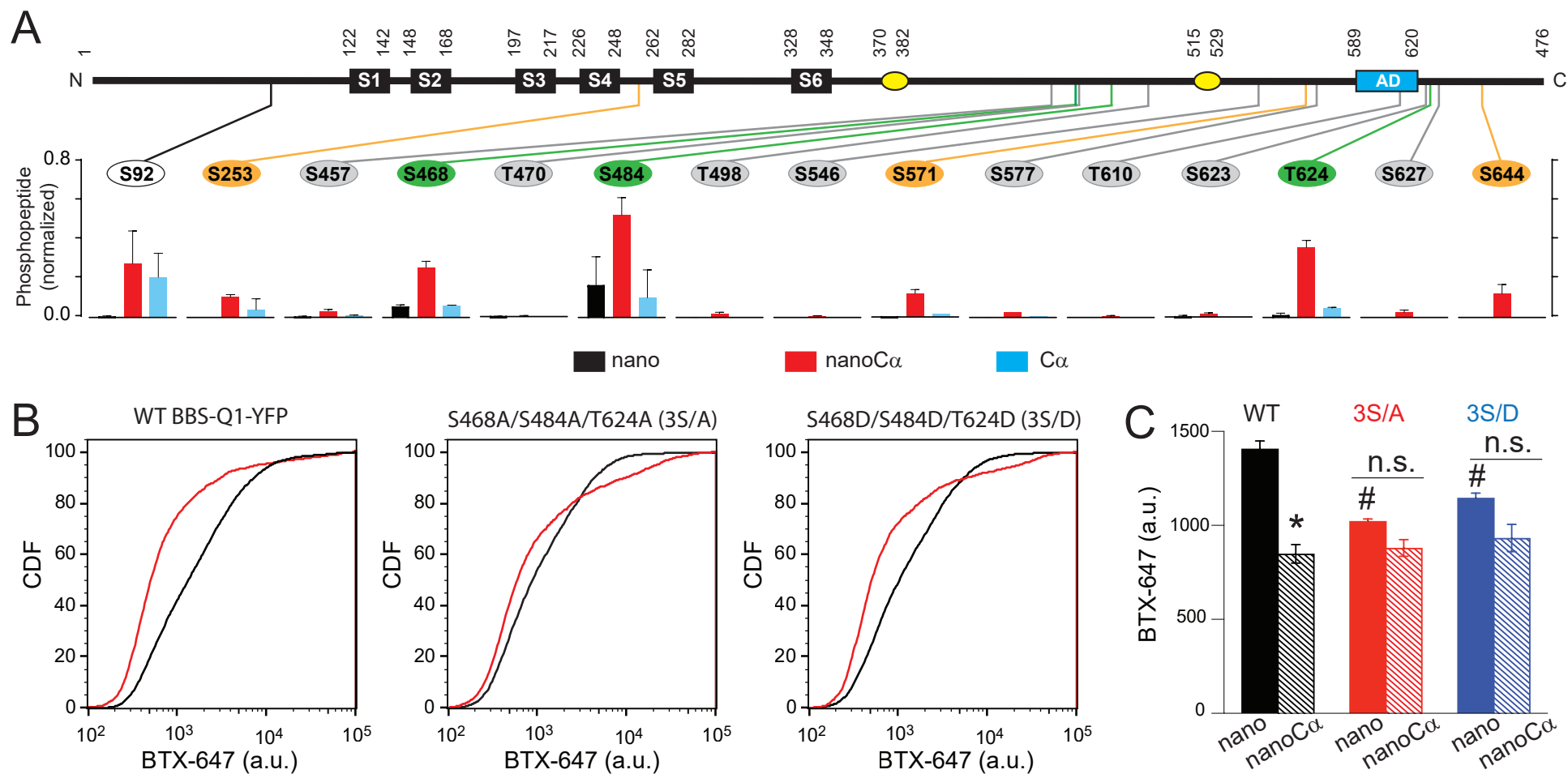
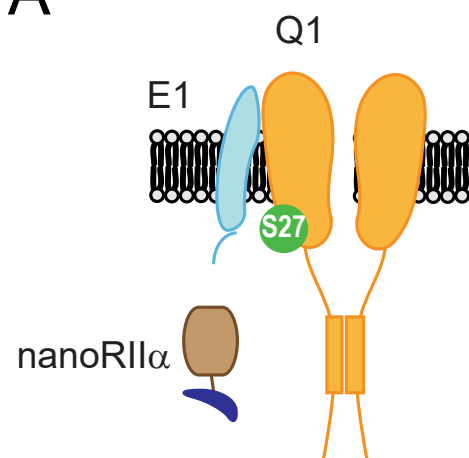


FIGURE 6

A



B

